PHILOSOPHICAL TRANSACTIONS OF THE ROYAL SOCIETY A MATHEMATICAL, PHYSICAL & ENGINEERING SCIENCES

Tunnel Structures as Probes of New Physics [and Discussion]

P. C. Main and P. D. Buckle

Phil. Trans. R. Soc. Lond. A 1996 **354**, 2311-2325
doi: 10.1098/rsta.1996.0102

Tunnel structures as probes of new physics

By P. C. Main

Department of Physics, University of Nottingham, Nottingham NG7 2RD, UK

The use of tunnelling and, in particular, resonant tunnelling devices to study basic physics is reviewed. Three principal areas are discussed. First, the use of tunnelling as an energy spectrometer to determine the energy levels in a quantum well. Specific applications of this include the energy levels of quantum dots and wires and the observation of the quantum mechanical energy levels of a classically chaotic system. Second, the application of a magnetic field perpendicular to the current (magneto-tunnelling spectroscopy) introduces a change in $\boldsymbol{k}$-vector of the tunnelling electron which allows the $\boldsymbol{k}$ dependence of the energy levels to be explored. This has been exploited in determining the dispersion of holes in quantum wells and in mapping the wavefunctions of electrons confined in quantum wires. Finally, it is possible to study tunnelling through localized states which exhibit effects due to electron–electron and electron–hole interactions, a regime which is difficult to investigate by other methods.

1. Introduction

The resonant tunnelling diode (RTD) was invented in 1974 by Chang, Esaki & Tsu (Chang *et al.* 1974) and there have been many applications, principally in the area of high-frequency electronics. The physics of the operation of the devices has been the subject of intense investigation but, in parallel with this, the RTD has also been used extensively as a microscopic laboratory for the study of fundamental phenomena in condensed matter physics. Although the use of tunnelling as a probe of physics is long established, for example to study energy gaps in superconductors by tunnelling through thin metal oxides, the GaAs–(AlGa)As heterostructures, which are the subject of this paper, have considerable advantages over other systems. First, modern growth techniques such as molecular beam epitaxy (MBE) allow the reproducible growth of very high quality layers with abrupt interfaces and high purity (Foxon, this issue). Second, the relatively low effective mass of electrons in the GaAs conduction band, $m^* = 0.07\,m_e$, where m_e is the bare electron mass, means that the tunnel barriers can be relatively wide without making the tunnel current too small. The separation between the initial and final tunnelling states is vital for the technique of resonant magneto-tunnelling spectroscopy which is described in § 2 below.

Figure 1*a* shows a schematic diagram of a typical double-barrier resonant tunnelling diode under applied bias. Electrical contact is made to the heavily doped n^+ regions but in most of the devices used in the experiments described in this paper, an undoped spacer layer is incorporated between the contacts and the (AlGa)As potential barriers. One effect of this is that the tunnelling into the well takes place from a two-dimensional electron gas (2DEG) formed in the triangular potential well at the emitter barrier as shown in the diagram. Application of a bias across the device raises

Phil. Trans. R. Soc. Lond. A (1996) **354**, 2311–2325
Printed in Great Britain

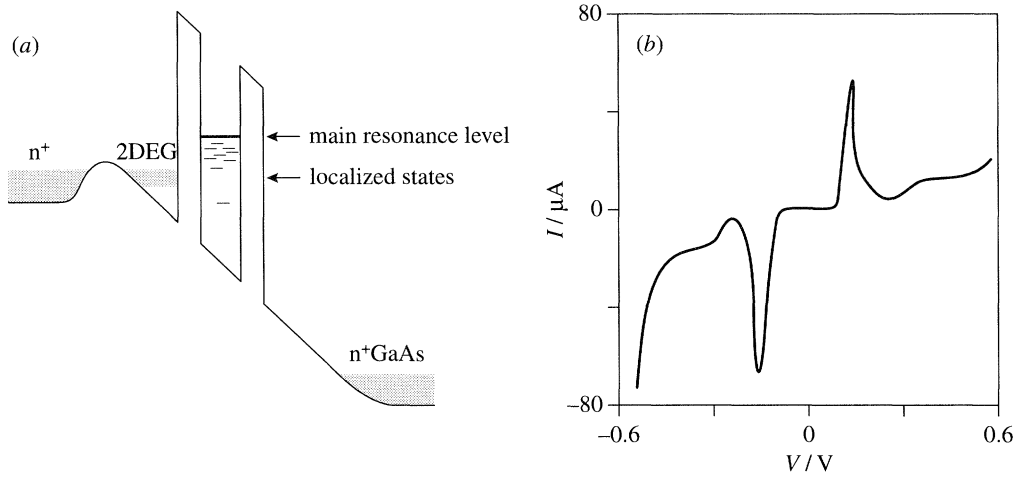

Figure 1. (*a*) Schematic diagram of the conduction band edge in a typical RTD under applied bias. The localized states are associated with impurities. (*b*) Typical low-temperature $I(V)$ characteristic for an RTD.

the energy of the 2DEG relative to states in the well. Due to conservation of in-plane momentum, there is resonant transmission of electrons from the emitter when the lowest energy electrons in the 2DEG are resonant with the continuum state of the well and this causes the onset of the well-known peak in the $I(V)$ characteristics of such devices (see figure 1*b*).

Section 2 describes in more detail the technique of resonant magneto-tunnelling spectroscopy (RMTS) and then in § 3–6 I discuss a variety of phenomena which have been studied using resonant tunnelling. The emphasis will be on a qualitative description of the experiments and how the tunnelling is used as a probe of fundamental physics. For further details, the reader is referred to the original publications.

2. Resonant magneto-tunnelling spectroscopy

Figure 1*b* illustrates that there is a peak in $I(V)$ whenever a state in the quantum well is resonant with the emitter 2DEG. At its most basic level this feature allows us to do spectroscopy on the energy levels of the well. For example, in p-type RTD it is possible to see resonances corresponding to both the heavy hole and light hole sections of the GaAs valence band (Hayden *et al.* 1991). The technique also allows the absolute energy scale of the levels to be determined from the bias across the device where a particular resonance occurs. Referring to figure 1*a*, the total bias is applied between the two electrical contacts but a fraction of it is dropped between the emitter and the quantum well. The numerical value of the fraction depends on the detailed form of the heterostructure but it may be calculated using simple electrostatic ideas (see, for example, Leadbeater 1990) or, in some cases, it may be determined from experiment. An example of the RTD as a spectrometer is outlined in § 3.

In zero magnetic field and in the absence of inelastic scattering, a tunnelling electron will conserve its $\boldsymbol{k}$-vector in the plane perpendicular to the tunnelling direction. Under these circumstances of translational symmetry, it is difficult to obtain information about the $\boldsymbol{k}$ dependence of the state in the well. However, the application of an in-plane magnetic field, i.e. perpendicular to the current direction, allows us to obtain information about $\boldsymbol{k}$. The principle of the technique is most easily understood

within a semiclassical framework (Leadbeater *et al.* 1988). An electron tunnelling in the z-direction subjected to a magnetic field B in the x-direction experiences a force which results in a change in k_y given by

$$\Delta k_y = (eB_x/\hbar) \int \nu_z \, \mathrm{d}t = (eB_x/\hbar)\Delta s, \tag{2.1}$$

where the time integral is over the tunnelling transition and Δs is the distance travelled by the tunnelling electron. In practice, this is taken to be the difference in positions between the maximum probability densities for the z-wavefunctions of the emitter and well states, respectively. The same result has been obtained quantum mechanically by treating the magnetic field as a perturbation (Davies *et al.* 1987). Equation (2.1) shows immediately why GaAs–(AlGa)As RTDs are so useful in this type of experiment. The magnitude of the shift in Δk_y is proportional to both B and Δs; the relatively wide barriers (typically *ca.* 6 nm) provide a useful range of Δk_y using readily accessible magnitudes of B which do not perturb the initial and final states substantially.

From equation (2.1), the application of an in-plane field allows the dispersion curve of states in the well to be determined—the technique of resonant magneto-tunnelling spectroscopy (RMTS). Furthermore, by rotation of the in-plane magnetic field it is possible to obtain dispersion in two dimensions in a given device. An excellent example of the use of this technique was provided by Hayden *et al.* (1991) in determining the hole dispersion in a quantum well using a p-type RTD. An example of their results is shown in figure 2. Note that they were able to identify anisotropy in the hole dispersion and also to tunnel into valence band states which were electron-like, i.e. with negative effective mass. RMTS is unique in its ability to measure these features.

3. Quantum chaology

The use of RTDs as spectrometers is highlighted in the experiments of Fromhold *et al.* (1994) which study the quantum mechanical energy levels of a classically chaotic system. The topic is of fundamental importance in that chaos is a classical phenomenon but there is a close relationship between the form of the quantum mechanical levels and particular unstable periodic orbits which are embedded in the sea of chaotic motion. Generally, there are rather few experimental systems in condensed matter where this relationship may be explored (Marcus *et al.* 1992; Weiss *et al.* 1993).

Fromhold *et al.* (1994) studied the tunnel current of an n-type RTD of the form shown in figure 1*a* but with a wide GaAs well, *ca.* 120 nm, sandwiched between two 5.6 nm wide $(Al_{0.4}Ga_{0.6})As$ barriers. In this system in zero magnetic field it is possible to observe literally dozens of resonances corresponding to the quantized states in the well, indicating that we are in the regime of high quantum number where it is sensible to consider classical analogues of the motion. In this case, the analogous classical system is a charged particle moving between two impenetrable walls in the presence of an electric field along the z-direction perpendicular to the walls. This is not a chaotic system. The application of a magnetic field either along z or perpendicular to z does not result in chaos either. However, when the magnetic field is applied at some angle θ relative to z then there is a wide range of values of θ and B where the classical motion is indeed chaotic and, in numerical simulations, the

PHILOSOPHICAL TRANSACTIONS OF THE ROYAL SOCIETY A MATHEMATICAL, PHYSICAL & ENGINEERING SCIENCES

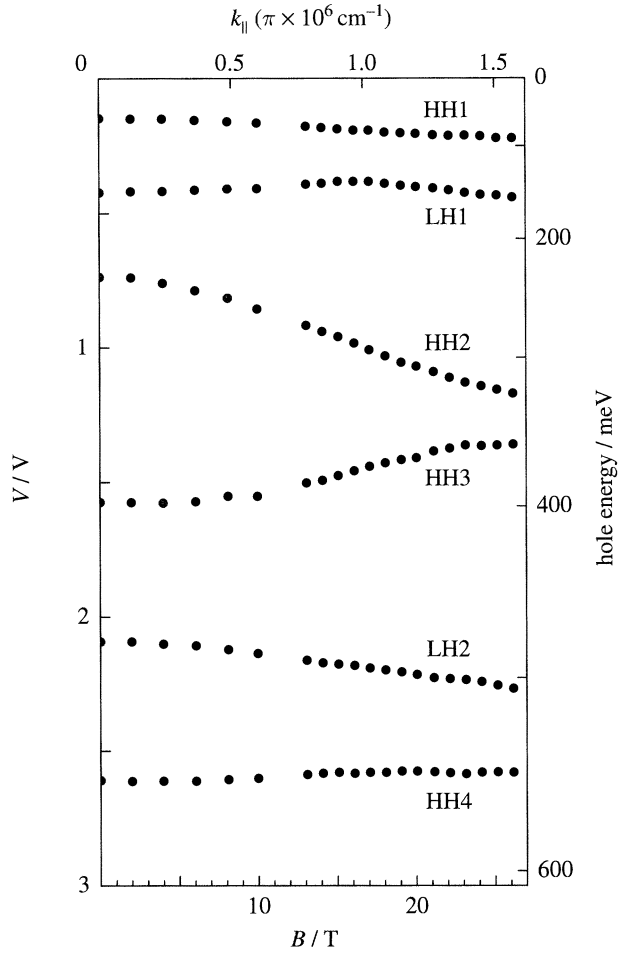

Figure 2. Valence band dispersion curves in a 4.2 nm wide quantum well showing heavy- (HH) and light-hole (LH) branches. The E and $k_{\|}$ axes are determined from V and B, respectively, as described in the text. Note the negative effective masses associated with, for example, HH3 (after Hayden *et al.* 1991).

motion of electrons appears to be random. However, within this sea of chaos, certain electrons with particular starting velocities do undergo precisely periodic motion which is unstable in the sense that another electron with slightly different velocity departs from this orbit at an exponential rate. According to Gutzwiller (1990), it is possible to predict certain properties of the quantum mechanical energy levels of the system by considering these classical orbits. In particular, in a complicated spectrum of energy levels typical of a classically chaotic system, periodic clusterings of levels occur. The energy spacings between clusters, ΔE, may be related to the periods of the unstable periodic orbits, T_{p}, by $\Delta E = h/T_{\mathrm{p}}$.

In the experiment, the energy levels in the well were determined from $I(V)$ in the usual way for a range of B and θ. In parallel, classical simulations identified the unstable periodic orbits. The initial velocities of the electrons in the simulations are chosen to be consistent with those of electrons which tunnel from the emitter 2DEG in the real device. Typical results are shown in figure 3 for $B = 11.4$ T and $\theta = 20°$. There are two series of levels, each with a distinct voltage period, labelled t and s.

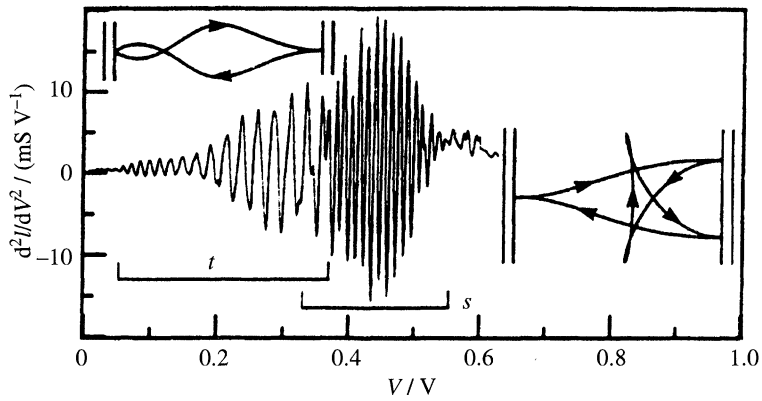

Figure 3. d^2I/dV^2 for a 120 nm wide quantum well in an 11.4 T magnetic field applied at 20° with respect to the current direction. The inset sketches represent the unstable periodic orbits, corresponding to the t and s series of oscillations, projected onto the x–y plane (after Fromhold *et al.* 1994).

The second derivative, d^2I/dV^2, is plotted to enhance the resonances relative to the smoothly varying background current. The voltage periods of the two series can be related, using the simple formula, to two unstable orbits in the simulation. One is a traversing (t series) orbit where the electron strikes the emitter and collector barrier consecutively. The other (s series) is a star-shaped orbit (shown projected onto the x–y plane as an inset to figure 3) where the electron strikes the collector barrier twice for each collision on the emitter barrier. Note that the experiments do not show clusters of levels but rather distinct individual peaks in the current. One of the reasons for this is that the RTD spectrometer has a natural limit to its resolution. Electrons injected into the well are 'hot' in that they have energies much higher than the bottom of the conduction band in the well. Therefore, they may relax by the emission of a longitudinal optic phonon with a lifetime $\tau_{\mathrm{LO}} \sim 0.2$ ps (Levi *et al.* 1987). It is impossible, therefore, to distinguish levels which are closer in energy than the linewidth imposed by this relaxation. The current oscillations in figure 3 may represent unresolved clusters of levels rather than individual levels (but see Fromhold *et al.* 1995*a*).

Since the simulation allows the 'tracking' of particular periodic orbits through different values of B, θ and V, it is possible to compare the predictions of the Gutzwiller formula with the experiment over a range of these variables. Such a plot is shown in figure 4 for the t and s series of figure 3 where B and θ are held constant. The solid experimental points are in good agreement with the open theory points calculated from the relevant unstable periodic orbits. There are no adjustable parameters. The flexibility of the experimental system has been shown by new studies of wells of different widths and also with the incorporation of impurities. For further details of this and related experiments see Fromhold *et al.* (1994, 1995*a*, *b*).

4. Wavefunction mapping

In § 2 the RMTS technique was described in terms of magnetic field perpendicular to the current causing a shift in the $\boldsymbol{k}$-vector when an electron tunnels between continuum states. There is a another recent application of this technique to tunnelling from a continuous, or quasi-continuous, emitter state into a localized state in the well.

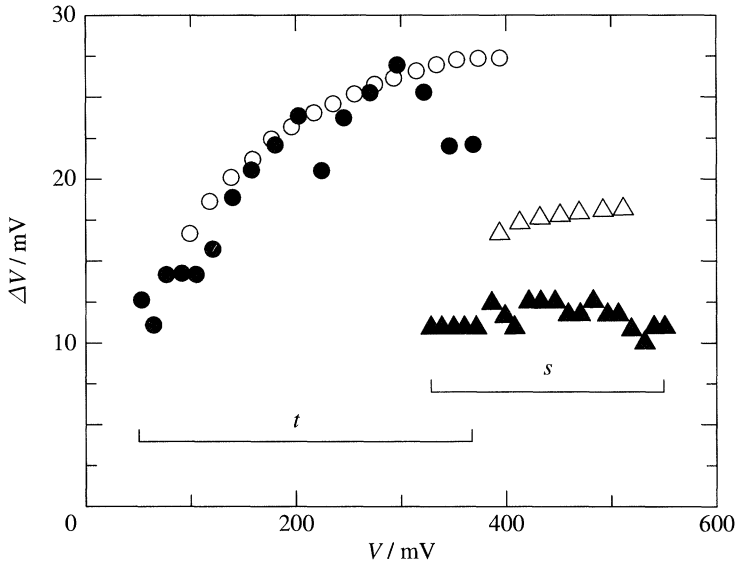

Figure 4. Variation of the period of the oscillations in $\mathrm{d}^2I/\mathrm{d}V^2$ shown in figure 3 versus applied bias. Open symbols are theory and the open ones are experimental (after Fromhold *et al.* 1994).

As discussed below, the shift in $\boldsymbol{k}$-vector introduced by the magnetic field in this case forms a unique probe of the form of the wavefunction in $\boldsymbol{k}$-space of the confined state, i.e. the Fourier transform of the real space wavefunction. To demonstrate this, consider the current due to tunnelling between an extended state in the emitter into a laterally confined state in the well. Taking the current direction as z, we make the assumptions: (i) that the 2D emitter is modelled using a Fang–Howard wavefunction (Fang & Howard 1966) and (ii) that the well state may be separated into the form

$$\Psi(x, y, z) = f(x)\, g(y)\, h(z). \tag{4.1}$$

The current density as a function of bias V and applied B along x is given using a Bardeen approach (Fromhold *et al.* 1992) by

$$I(V, B) = \frac{-2em^*}{\pi\hbar^3} \int_{\Delta k - k_c}^{\Delta k + k_c} \frac{|M(k_y, k_v)|^2}{k_v} \mathrm{d}k_y, \tag{4.2}$$

where $M(k_y, k_x)$ is proportional to the tunnelling transition rate and is determined primarily by the overlap integrals between the lateral (i.e. x, y) part of the initial and final wavefunctions.

$$M \propto \int_{-\infty}^{+\infty} \int_{-\infty}^{+\infty} \mathrm{e}^{\mathrm{i}k_x x} \mathrm{e}^{\mathrm{i}k_y y} g(y)\, f(x)\, \mathrm{d}x\, \mathrm{d}y \propto F(k_x)\, G(k_y) \tag{4.3}$$

in the case where the initial state is a plane wave and $G(k_y)$ and $F(k_x)$ are the Fourier transforms of $g(y)$ and $f(x)$, respectively. Δk is given by equation (2.1); $k_c = k_c(V)$ is the maximum value of k_y consistent with energy conservation at a particular voltage and k_v, defined by $k_v^2 = k_c^2 - (k_y - k_0)^2$, is the particular value of k_x which is allowed by energy conservation for a value of k_y. The calculation of equation (4.2) assumes that the amplitudes of the initial and final wavefunctions within the barriers are not perturbed by the applied magnetic field. In this approximation, therefore, the amplitude of the current corresponding to tunnelling from a 2DEG into a localized

state will vary with B applied along x according to

$$I(V_\mathrm{p}, B)/I(V_\mathrm{p}, 0) = |G(\Delta k)|^2/|G(0)|^2, \tag{4.4}$$

where V_p is the bias at which the $k = 0$ state in the emitter is aligned with the energy of the localized state in the well, i.e. when k_c is very small. To a good approximation this is when the current from the emitter into the localized state is maximum (Fromhold *et al.* 1992). In other words, the variation of the peak current in $I(V)$ with the magnitude of B applied along x is proportional to the square of the Fourier transform of the lateral wavefunction in the y-direction.

Two experiments have been performed using this technique. In the first, the confined state in the well is provided by a donor impurity (Sakai *et al.* 1993). A δ-layer of donor impurities ($4 \times 10^{13}\ \mathrm{m}^{-2}$) was incorporated into the centre plane of the quantum well of a RTD. At this concentration, the donor impurities in the well have an average separation much larger than the Bohr radius of a bound electron state so they may be considered largely independent (but see § 5). A clear feature in $I(V)$ was observed due to tunnelling from the emitter 2DEG into these shallow donor states. Measurement of the amplitude of this peak as a function of applied B enabled information to be obtained about the donor wavefunction in the well. However, in this case the applied magnetic field also distorts the wavefunction of the confined state and the analysis of the data is not straightforward because $g(y)$ itself depends on B.

The second example is more clear cut (Wang *et al.* 1994*a*; Beton *et al.* 1995). Here the confinement was produced by using a novel optical lithography and wet etching technique to produce one-dimensional states in the well. The device is shown schematically in figure 5*a*. The wafer was grown by MBE to the standard pattern but, for reasons concerned with the fabrication technique (for full details, see Wang *et al.* 1994*b*) the 4.7 nm wide barriers were AlAs. The GaAs quantum well is 9.0 nm across. The active region of the device is defined by the top contact which has dimensions $\ell_\mathrm{t} \times \ell_\mathrm{b} = 0.5\,\mu\mathrm{m} \times 1.0\,\mu\mathrm{m}$ but sidewall depletion, shown by the dashed curve in figure 5*a*, means that the dimensions of the conducting area are more likely to be *ca.* 50 nm × 600 nm. For the experiment of interest here, the electrons travel from the bottom contact to the top contact. A schematic profile of the conduction band edge, with the device under bias, is shown in figure 5*b*. The lateral confinement induced by the small dimension ℓ_t is assumed to be parabolic which means that the electron energy levels are $E_i = E_0 + (i + \frac{1}{2})\hbar\omega_\mathrm{e}$ for the ith state in the emitter and $E_j = E_1 + (j + \frac{1}{2})\hbar\omega_\mathrm{w}$ for jth state in the well, where we have assumed parabolic confinement and the notation follows the diagram. For this device the sidewall depletion means that $\hbar\omega_\mathrm{e} < \hbar\omega_\mathrm{w}$, i.e. the electrons in the well are more confined than those in the emitter. Despite this, in the voltage range of interest only the $i = 0$ emitter level is occupied and tunnelling may occur into any of the j subbands, depending on applied bias.

$I(V)$ at $T = 0.3\,\mathrm{K}$ is shown in figure 6 with the resonances marked in terms of the j index 0 and 2 (both transitions from $i = 0$). The $i = 0$ to $j = 1$ resonance is forbidden because the initial and final states have different parity. Note the form of $I(V)$ is very different to that of a bulk device. Similar peaks have been seen by many authors in a variety of submicron RTD but the RMTS technique not only proves that these resonances are due to tunnelling through laterally confined states but it also allows mapping of the state wavefunctions. As usual the magnetic field is applied perpendicular to the current, in this case parallel to the longer dimension ℓ_b. The effect of the field is also shown in figure 6. The amplitude of the $j = 0$ resonance

PHILOSOPHICAL TRANSACTIONS OF THE ROYAL SOCIETY A MATHEMATICAL, PHYSICAL & ENGINEERING SCIENCES

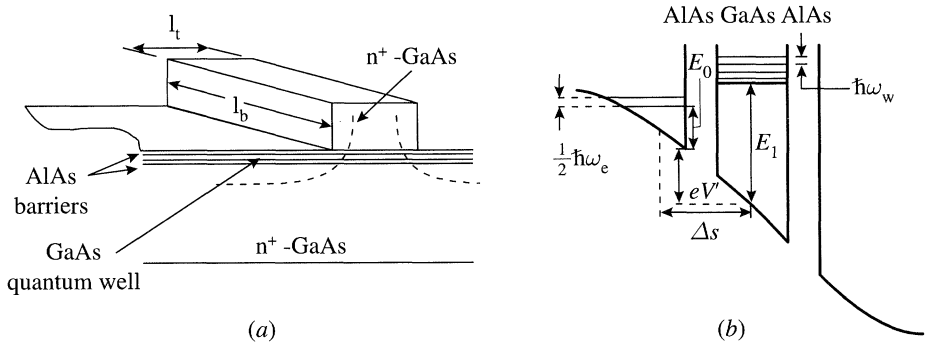

Figure 5. (*a*) Schematic diagram of a one-dimensional RTD fabricated by optical lithography and wet etching. The dashed curve represents the boundary of the depletion region. (*b*) Conduction band edge of the device under bias. See the text for an explanation of the symbols.

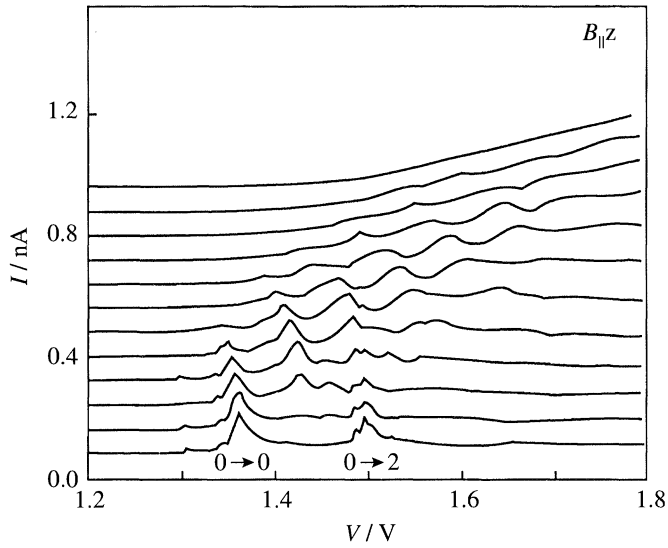

Figure 6. $I(V)$ at 300 mK for the device shown in figure 5 at magnetic fields from 0 T (bottom) to 10 T (top) in 1 T steps. The labels $0 \rightarrow 0$ and $0 \rightarrow 2$ refer to $i \rightarrow j$ transitions between 1D states in the emitter and well. The curves are offset for clarity.

decreases monotonically with decreasing field whereas the $j = 2$ amplitude first decreases then increases again before dying away. Note the $j = 1$ resonance is no longer forbidden in a finite B but at high field its amplitude also decays away.

Strictly speaking, equation (4.3) is valid only for plane wave states in the emitter whereas in this case there is one-dimensional confinement in both the emitter and the well. However, since $\hbar\omega_e < \hbar\omega_w$, it is still approximately valid (see below). Figure 7 shows the amplitude of the three resonances as a function of B. The curves are displaced for clarity. The theoretical values of the squares of the Fourier transforms (FT) of the corresponding harmonic oscillator states are shown as solid curves. The parameter k_y is Δk of equation (2.1), the shift induced by B and $k_w = (m^*\omega_w/\hbar)^{1/2}$ is the natural wavevector for a harmonic oscillator. Comparing the two curves gives $\hbar\omega_w = 10\,\text{meV}$ which is also consistent with the voltage spacing of the resonances at $B = 0$. The effect of the confinement in the emitter can be seen in the slight smearing of the FT of the $j = 2$ state but it is clear that the essential mapping

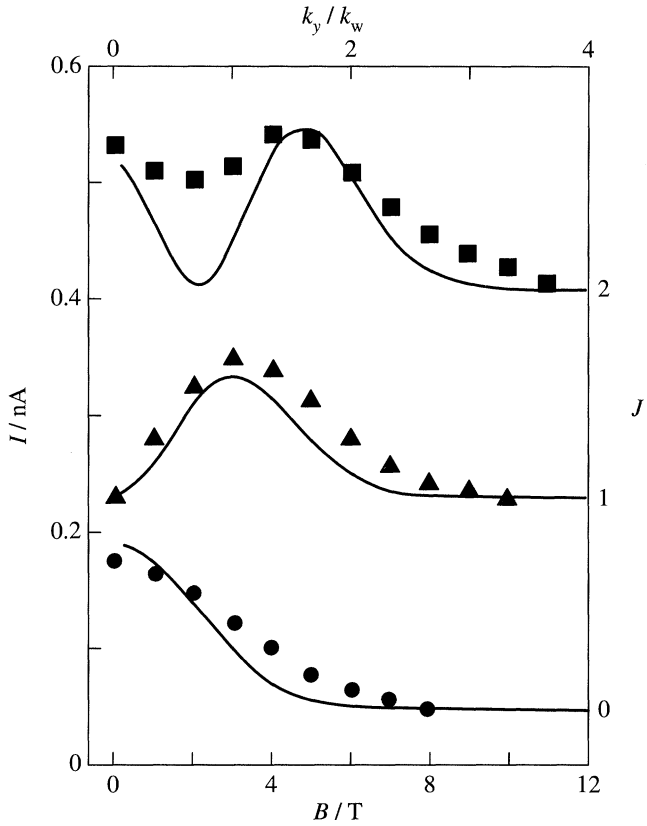

Figure 7. $I(B)$ for the peak current at the $0 \rightarrow 0, 0 \rightarrow 1$ and $0 \rightarrow 2$ transitions. Discrete points are experimental and the solid curves represent the squares of the Fourier transforms of the three lowest energy states of a harmonic oscillator. Curves are offset for clarity. The determination of the $\boldsymbol{k}$-axis is described in the text.

of the wavefunction is not affected. More careful analysis gives $\hbar\omega_e \simeq 5\,\text{meV}$ or $\hbar\omega_e = \hbar\omega_w/2$. For further details of this investigation and other experiments on similar devices see Wang *et al.* (1994*a*) and Beton *et al.* (1995).

5. Interaction effects and mesoscopics

There is a history of tunnelling being used to explore the density of states in a conductor where there are interactions between carriers. In semiconductors, low-temperature tunnelling between parallel 2D electron or hole systems has provided evidence for the existence of energy gaps at the Fermi energy which are a consequence of carrier–carrier interactions (see, for example, Murphy *et al.* 1994). Recently, Geim *et al.* (1994*a*), showed that there was another regime where tunnelling could give information about interaction effects. In this experiment the interaction occurred between the 2DEG accumulated at the emitter barrier of a RTD and a single unscreened tunnelling electron.

The device was a standard RTD but with a δ-layer of donor impurities (2×10^{13}–$8 \times 10^{13}\,\text{m}^{-2}$) incorporated at the centre plane of the quantum well. For full sample details see Sakai *et al.* (1993). The effect of these impurities is to form a set of localized electronic states at energies below that of the first continuum state of the quantum

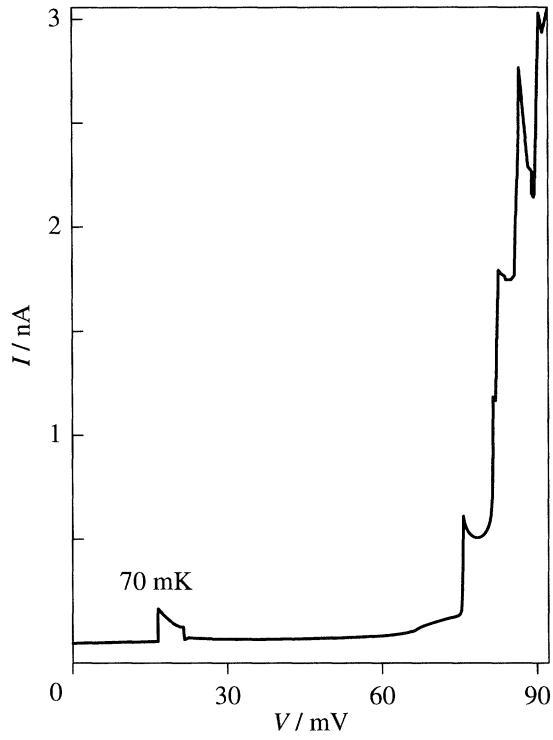

Figure 8. The onset of $I(V)$ for a RTD 12 μm across (after Geim *et al.* 1994*a*).

well, as shown in figure 1. The first continuum resonance in $I(V)$ is largely unaffected by the introduction of these impurities although for large impurity concentrations an extra feature does occur at biases lower than that of the main resonance. This has been shown to be due to tunnelling through electron states associated with isolated shallow donors and is called the single-donor resonance (SDR) (Sakai *et al.* 1993). However, at even lower biases it is possible to see well-defined peaks in $I(V)$ but on a current scale many orders of magnitude smaller than that of the continuum resonance. An example of such a structure is shown in figure 8 for a RTD in the form of a square mesa of lateral dimension 12 μm. Similar structure at low bias has been seen in all devices of this type and, indeed, in all RTD where the current resolution is sufficiently high. Even in devices with no intentional doping there are usually sufficient accidental impurities to create similar features although the amount of structure is roughly proportional to the number of impurities. In nominally identical devices, the structure is always qualitatively similar but different in detail, characteristic of a mesoscopic system.

This subthreshold structure is due to tunnelling through localized states associated with clusters of donors in the well which are formed by random chance (Geim *et al.* 1994*b*). These create electron states with up to two or three times the binding energy of isolated donors and hence lead to structure in $I(V)$ at lower biases than the SDR. The feature at *ca.* 26 mV in figure 8 is due to a single state in the well and, correspondingly, due to the passage of electrons one at a time through the quantum well. The localized character of the state (*ca.* 10 nm) means that only one electron may occupy the site at any one time. The current associated with the passage of the single electron, *ca.* 100 pA, is consistent with the expected lifetime of the state.

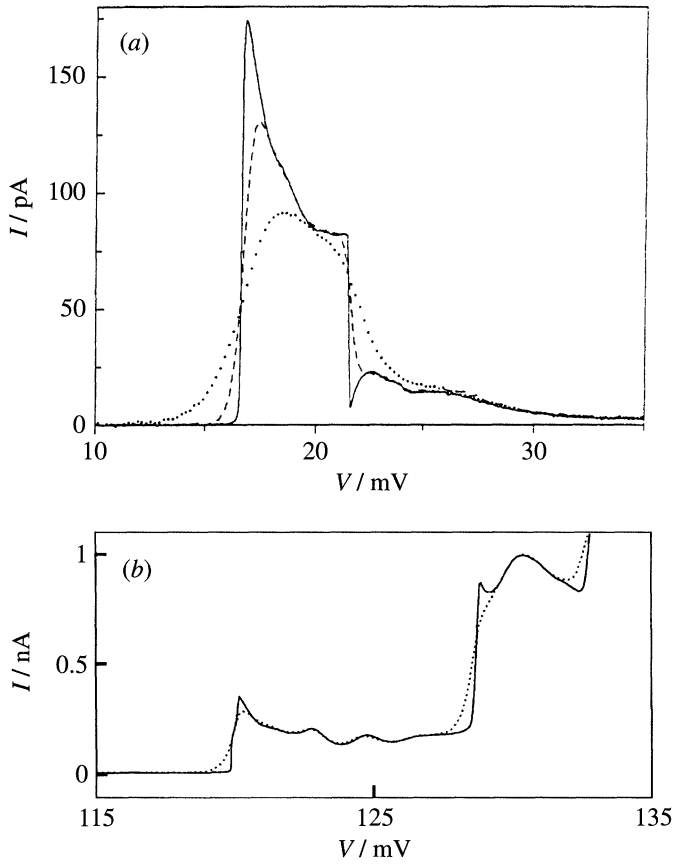

Figure 9. (*a*) The lowest bias feature of figure 8 at $T = 70$ mK (solid curve), 1.3 K (dashed curve) and 5 K (dotted curve) (after Geim *et al.* 1995). (*b*) $I(V)$ near the current onset for a 6 μm wide RTD for two temperatures.

It is interesting to consider the temperature dependence of the structure in $I(V)$ shown in figure 8. Figure 9*a* shows the single feature at three different temperatures. As temperature decreases, it is striking to note the singular enhancement of the tunnel current at the onset of the feature, which corresponds to the situation where the localized state is resonant with the Fermi energy of the emitter 2DEG. This was the first observation of a 'Fermi edge singularity' (FES) in a transport experiment, although similar effects are commonly used to explain features in optical properties of metals and doped semiconductors (see, for example, Nash *et al.* 1993).

The origin of the FES is the strong interaction between the tunnelling electron and the emitter 2DEG. The unique feature of the RTD here is that the current is sensitive to the passage of just this one electron; there is no smearing due to averaging over a large number of states. Therefore, the tunnel current measures directly the singularity in the transmission coefficient due to the interactions. In simple terms the FES is a result of second-order processes, whereby the tunnelling electron need not conserve energy because any excess or deficiency can be made up by scattering of electrons in the 2DEG. Thus an electron may tunnel into the localized site from an initial state which would not be allowed in a model of non-interacting particles. As yet, there is no complete theory for the form of the FES. Although Matveev & Larkin (1992) deal

with a similar physical situation to the experiment, their theory is for weak coupling between the 2DEG and the tunnelling electron, $\lambda_F/d \ll 1$, where d is the spatial separation of the 2DEG and the localized state and λ_F is the Fermi wavelength in the 2DEG. In the experiment $\lambda_F/d > 1$; nevertheless, it is possible to fit the form of the experimentally measured FES to the theory (Geim *et al.* 1994*a*) but the variety of the forms of the FES observed means that there is still a considerable amount of work to be done in understanding this system.

Although there is considerable variation in the form of the FES in different devices, they are not at all uncommon. Figure 9*b* shows the FES in another device, this one with lateral dimension 6 μm. $I(V)$ is shown for $T = 900$ mK and 100 mK. This is a typical curve in that it shows that near onset, the current increases in a series of thermally activated steps (two are visible in this figure), each accompanied by a FES. However, the steps are separated by a regions of $I(V)$ which are strictly independent of temperature over the range illustrated. Each step is associated with a different localized state in the well. It follows, therefore, that the temperature-independent structure must be associated with a property of the emitter 2DEG. It is possible that it may be associated with plasmon effects, analogous to those calculated for the optical case (Hawrylak 1991). However, the variation of the structure under the application of a magnetic field (McDonnell *et al.* 1995) would appear to rule this out. More likely, the current fluctuations represent fluctuations in the density of states as a result of quantum interference in the disordered emitter 2DEG (McDonnell *et al.* 1995; Schmidt *et al.* 1995; Sivan *et al.* 1994). In this case the localized state in the well is being used as a local probe of the 2DEG.

Another example of the use of a RTD to explore interaction effects has been the fabrication of RTD with submicron lateral dimensions (Reed *et al.* 1988). Although it has proved difficult to show unambiguously the presence of three-dimensional quantum confinement (but see § 4) in the $I(V)$ of such devices, it has been possible to show reproducible Coulomb blockade effects (Su *et al.* 1992; Tewordt *et al.* 1992; Nogaret *et al.* 1995) where it is possible to control the number of electrons in the quantum well either by varying the bias or applying a magnetic field. In this case it is necessary to have RTD which have asymmetric barriers so that the transmission through one barrier is much less than the other to allow charge build-up in the quantum well. Unlike the experiments in lateral, gated 2DEG systems (Meirav *et al.* 1989) in the RTD quantum dot the number of electrons in the dot is known precisely and, furthermore, may be increased from zero. Figure 10 shows an example (Nogaret *et al.* 1995) of tunnelling through a laterally confined quantum dot where the lateral dimension of the active region is *ca.* 40 nm. In zero magnetic field the number of electrons in the dot is determined by the applied bias; however, the application of a magnetic field, this time parallel to the current, causes a diamagnetic shift in the energy of the states in the well causing a depopulation of these states. For the upper curve, where there are originally two electrons in the dot, the current falls to a value consistent with there being just one electron there and, with a further increase in field, the current falls to zero. The spacing of the current steps in B and with respect to the applied bias indicate that the capacitance between the dot and the electrical contacts is *ca.* 0.14 fF. These experiments also indicate that it may be possible to probe the energy of systems involving very small numbers of electrons and, in particular, to test the many-body theoretical predictions for the energy levels of such interacting systems (e.g. Maksym 1993). At present there is no other experiment which allows this flexibility.

PHILOSOPHICAL TRANSACTIONS OF THE ROYAL SOCIETY A MATHEMATICAL, PHYSICAL & ENGINEERING SCIENCES

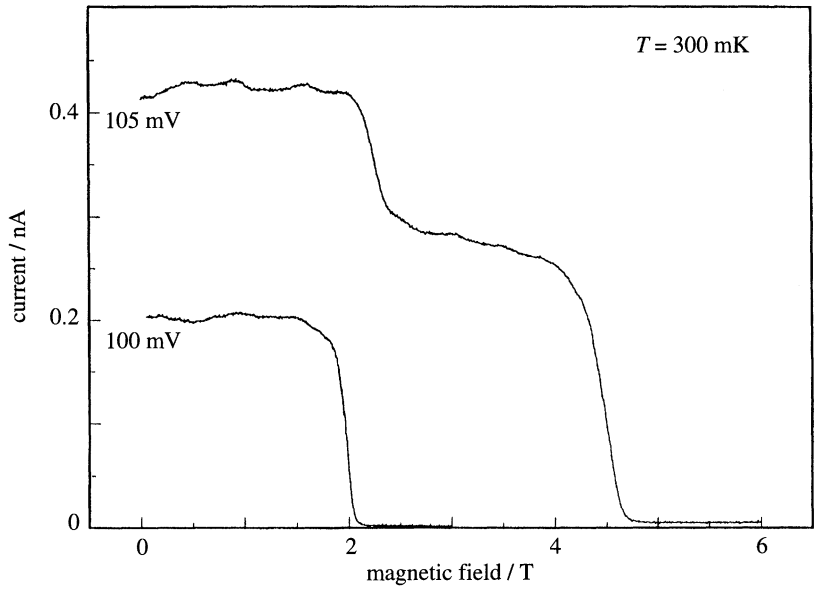

Figure 10. Magnetic field controlled Coulomb blockade in an asymmetric RTD at 300 mK. Each curve is at a different applied bias. The current steps correspond to either one or two electrons in the quantum well. The zero-dimensional state in the quantum well has a radius *ca.* 40 nm (after Nogaret *et al.* 1995).

6. Conclusions and prospects

The GaAs–(AlGa)As RTD is the ideal system to use tunnelling to explore qualitatively new physics. The RMTS technique allows the $\boldsymbol{k}$ dependence of the states in the well to be probed in addition to their energy dependence which is the natural result of a resonant tunnelling experiment. This procedure has a unique application to localized states where the form of their wavefunctions may be determined. Note that the technique is complementary to the use of scanning probe microscopy to investigate the wavefunctions of surface states (Crommie *et al.* 1993). In the future it should be possible to study the wavefunctions of other types of structure, such as superlattices, which may be embedded in a RTD.

The use of RTD to look at effects due to impurities is now well established. Tunnelling through a single impurity state allows us to probe a new regime of strongly interacting electrons where the tunnelling channel is self-organized by the statistical effects of disorder (Geim *et al.* 1994*b*). Other systems are also possible, for example parallel electron–hole gases in p–i–n structures, where tunnelling can provide information about the excitonic states. Conversely, the localized states may also be used as probes of the emitter states and recently there have been attempts (Nogaret *et al.* 1995) to investigate the density of states of submicron, ring-shaped emitters to search for quantum coherent effects. In principle, this idea may be employed to study a wide range of properties in the 2DEG, such as localization, mobility edge, Coulomb gap, chaos etc. With the prospect of new ultra-small systems, such as self-organized InAs dots, the techniques described above form a powerful tool in extracting important information about the electron states associated with these objects.

This review represents the work of many people in the Department of Physics at the University of Nottingham. I am particularly grateful for the assistance of Laurence Eaves, Peter Beton and Mark Fromhold. This work is supported by EPSRC(UK).

References

Beton, P. H., Wang, J., Mori, N., Eaves, L., Main, P. C., Foster, T. J. & Henini, M. 1995 *Phys. Rev. Lett.* **75**, 1996.

Chang, L. L., Esaki, L. & Tsu, R. 1974 *Appl. Phys. Lett.* **24**, 593.

Crommie, M. F., Lutz, C. P. & Eigler, D. 1993 *Nature* **363**, 524.

Davies, R. A., Newson, D. J., Powell, T. G., Kelly, M. J. & Myron, H. W. 1987 *Semicond. Sci. Technol.* **2**, 61.

Fang, F. F. & Howard, W. E. 1966 *Phys. Rev. Lett.* **16**, 797.

Fromhold, T. M., Sheard, F. W. & Eaves, L. 1992 *Acta. Phys. Pol.* A **82**, 737.

Fromhold, T. M., Eaves, L., Leadbeater, M. L., Foster, T. J. & Main, P. C. 1994 *Phys. Rev. Lett.* **72**, 2608.

Fromhold, T. M., Wilkinson, P. B., Sheard, F. W., Eaves, L., Miao, J. & Edwards, G. 1995*a* *Phys. Rev. Lett.* **75**, 1142.

Fromhold, T. M., Fogarty, A., Eaves, L., Sheard, F. W., Henini, M., Foster, T. J. & Main, P. C. 1995*b* *Phys. Rev.* B **51**, 18 029.

Geim, A. K., Main, P. C., La Scala Jr., N., Eaves, L., Foster, T. J., Beton, P. H., Sakai, J. W., Sheard, F. W., Henini, M., Hill, G. & Pate, M. A. 1994*a* *Phys. Rev. Lett.* **72**, 2061.

Geim, A. K., Foster, T. J., Nogaret, A., Mori, N., McDonnell, P. J., La Scala Jr., N., Main, P. C. & Eaves, L. 1994*b* *Phys. Rev.* B **50**, 8074.

Gutzwiller, M. C. 1990 Chaos in classical and quantum mechanics. New York: Springer.

Hawrylak, P. 1991 *Phys. Rev.* B **44**, 3821.

Hayden, R. K., Maude, D. K., Eaves, L., Valaradares, E. C., Henini, M., Sheard, F. W., Hughes, O. H., Portal, J. C. & Cury, L. 1991 *Phys. Rev. Lett.* **66**, 1749.

Leadbeater, M. L., Eaves, L., Simmonds, P. E., Toombs, G. A., Sheard, F. W., Claxton, P. A., Hill, G. & Pate, M. A. 1988 *Solid State Electron.* **31**, 707.

Leadbeater, M. L. 1990 Ph.D. thesis, University of Nottingham.

Levi, A. F. J., Späh, R. J. & English, J. H. 1987 *Phys. Rev.* B **36**, 9402.

Maksym, P. A. 1993 *Physica* **184B**, 385.

Marcus, C. M., Rimberg, A. J., Westervelt, R. M., Hopkins, P. F. & Gossard, A. C. 1992 *Phys. Rev. Lett.* **69**, 506.

Mateev, K. A. & Larkin, A. I. 1992 *Phys. Rev.* B **46**, 15 337.

McDonnell, P. J., Geim, A. K., Main, P. C., Foster, T. J., Beton, P. H. & Eaves, L. 1995 *Physica* **211B**, 433.

Meirav, U., Kastner, M. A., Heiblum, M. & Wind, S. J. 1989 *Phys. Rev.* B **40**, 5871.

Murphy, S. Q., Eisenstein, J. P., Boebinger, G. S., Pfeiffer, L. N. & West, K. W. 1994 *Phys. Rev. Lett.* **72**, 728.

Nash, K. J., Skolnick M. S., Saker, M. K. & Bass, S. J. 1993 *Phys. Rev. Lett.* **70**, 3115.

Nogaret, A., Gompertz, M. J., Main, P. C., Eaves, L., Foster, T. J., Henini, M. & Beaumont, S. P. 1996 Proc. EP2DSXI *Surf. Sci.* **361/2**, 644.

Reed, M. A., Randall, J. N., Aggarwal, R. J., Matyi, R. J., Moore, T. M. & Wetsel, A. E. 1988 *Phys. Rev. Lett.* **60**, 535.

Sakai, J. W., Fromhold, T. M., Beton, P. H., Eaves, L., Henini, M., Main, P. C., Sheard, F. W. & Hill, G. 1993 *Phys. Rev.* B **48**, 5664.

Schmidt, T., Haug, R. J., Fal'ko, V. I., von Klitzing, K., Förster, A. & Lüth, H. 1995 Preprint.

Sivan, U., Milliken, F. P., Millikove, K., Rishton, S., Lee, Y., Hong, J. M., Boegli, V., Kern, D. & DeFranza, M. 1994 *Europhys. Lett.* **25**, 605.

Su, B., Goldman, V. J. & Cunningham, J. E. 1992 *Phys. Rev.* B **46**, 764.

Tewordt, M., Martín-Moreno, L., Nicholls, J. T., Pepper, M., Kelly, M. J., Law, V. J., Ritchie, D. A., Frost, J. E. F. & Jones, G. A. C. 1992 *Phys. Rev.* B **45**, 14 407.

Wang, J., Beton, P. H., Mori, N., Eaves, L., Buhmann, H., Mansouri, L., Main, P. C., Foster, T. J. & Henini, M. 1994*a* *Phys. Rev. Lett.* **73**, 1146.

PHILOSOPHICAL TRANSACTIONS OF THE ROYAL SOCIETY A MATHEMATICAL, PHYSICAL & ENGINEERING SCIENCES

Wang, J., Beton, P. H., Mori, N., Buhmann, H., Mansouri, L., Eaves, L., Main, P. C., Foster, T. J. & Henini, M. 1994*b* *Appl. Phys. Lett.* **65**, 1124.

Weiss, D., Richter, K., Menschig, A., Bergmann, R., Schweizer, H., von Klitzing, K. & Weimann, G. 1993 *Phys. Rev. Lett.* **70**, 4118.

Discussion

P. D. Buckle (*Department of Electrical Engineering and Electronics, University of Manchester Institute of Science and Technology (UMIST), UK*). In the wavefunction mapping experiments, have $I(V)$ measurements been performed in the reverse bias direction? If so, with reference to the theory curve plotted for the $n = 2$ wavefunction, and the slight disagreement with that experimentally observed, was the agreement worse in the reverse bias direction due to reduced dimensionality in the reverse bias emitter states?

P. C. Main. The reverse bias characteristics of this device did not show the resonances seen in forward bias, although the wafer from which the device is made is nominally symmetric. The reason for this is that the processing introduces asymmetry, as is evident from the different lateral confinement in the emitter and the quantum well. In reverse bias, we believe the electrostatic potential is such that when the bias is high enough to form an emitter accumulation layer, it is beyond the resonances. We see the inelastic peak due to longitudinal optic phonons in reverse bias.

Note that the wavefunction mapping technique relies on one of the wavefunctions being more localized than the other. If the emitter wavefunction were more localized in reverse bias than in forward bias we would indeed expect to lose information about the wavefunction in the quantum well.

PHILOSOPHICAL TRANSACTIONS OF THE ROYAL SOCIETY A MATHEMATICAL, PHYSICAL & ENGINEERING SCIENCES